Effect of super vacuum assisted high pressure die casting on the repeatability of mechanical properties of Al-Si-Mg-Mn die-cast alloys

Xixi Dong, Xiangzhen Zhu, Shouxun Ji *
Brunel Centre for Advanced Solidification Technology (BCAST), Brunel University London, Uxbridge, Middlesex UB8 3PH, United Kingdom
*Corresponding author: Tel: +44 1895 266663; Fax: +44 1895 269758
E-mail address: shouxun.ji@brunel.ac.uk

Abstract

Two-stage super vacuum (19 mbar) assisted high pressure die casting (HPDC) was achieved by evacuating from the die cavity and the shot sleeve simultaneously. The effect of super vacuum assisted HPDC on the repeatability of the tensile properties of Al-Si-Mg-Mn die-cast alloy was investigated in comparison with conventional HPDC. The quantitative Weibull analysis confirmed that super vacuum assisted HPDC improved the repeatability of the tensile properties of the alloy. The data and deviation analysis verified that super vacuum assisted HPDC considerably decreased the fluctuations of the ductility of the alloy by 71 % in as-cast state and 84 % after solution and ageing treatment. The results also showed that super vacuum assisted HPDC improved the ultimate tensile strength and ductility of the as-cast alloy by 5.6 % and 43 %, respectively, and increased the ductility of the alloy by 21 % after solution and ageing treatment. The significant improvements of ductility and the repeatability of tensile properties were originated from the decrease of porosity volume fraction and porosity size in the alloy processed by super vacuum assisted HPDC. The reduction of defect size can improve the stress distribution and retard the crack initiation in castings. Therefore, the tensile strength and ductility were enhanced in the die-cast alloy processed by super vacuum assisted HPDC.

Key words: Aluminium alloys; High pressure die casting; Vacuum; Microstructure; Mechanical properties; Repeatability.

1. Introduction

As a near-net shape manufacturing process, high pressure die casting (HPDC) is very attractive in producing thin-wall components with high dimensional accuracy, high production efficiency and considerable economic benefits for automotive and other industries. However, conventional HPDC castings usually contain randomly distributed gas porosities mainly due to the entrapment of gas under the high-speed shot. Wang et al. (2011) studied the content of gas in the castings made by HPDC. Li et al. (2016) investigated the defect of porosity in the AM60B magnesium alloy processed by HPDC and its effect on the fracture. An electromagnetic transport (EMT) process was reported for HPDC (Dong et al., 2015; Dong et al., 2016). The EMT process could decrease the porosity in A380 die-cast aluminium alloy, as reported by Dong et al. (2015). The defect of porosity was detrimental to the tensile properties of HPDC components (Niu et al., 2000), resulting in the application of large safety factor in component design and thus reducing the potential of weight-saving of thin-wall components. Moreover, the formed gas porosities in die-castings were expanded in size at elevated temperatures, which resulted in the blisters on the surface of castings during solution treatment (Wan et al., 2013). Therefore, the component made by conventional HPDC was hard to be strengthened by the solution and ageing heat treatment.

Various techniques have been applied to decrease the level of porosity in castings made by HPDC. Ji et al. (2013) reported the decrease of porosity in the die-cast AM60 magnesium alloy under the treatment of melt conditioning. Wang et al. (2014) reported the improvement of porosity in the die-cast AZ91 magnesium alloy under vacuum assisted HPDC. The application of vacuum in HPDC process is promising for the significant reduction of the gas entrapment during die filling. Patel et al. (2012) reported the improvement of the deformation capability of castings under vacuum assisted HPDC. Wen et al. (2012) reported the enhanced property of fatigue of castings processed by vacuum assisted HPDC. Li et al. (2016) reported the increase of tensile properties in the AZ91D alloy under vacuum assisted HPDC. Cao et al. (2017) reported the effect of vacuum levels on the castings made by HPDC. However, the benefits under vacuum assisted HPDC are still not well understood and developed. Limited information can be found for the quantitative relationship between the decrease of porosity and the improvement of mechanical properties under vacuum assisted HPDC. On the other hand, one of the main concerns in die castings is the large uncertainty and fluctuation of mechanical

properties in individual casting, due to the random and irregular distribution of porosities in castings, as reported by Lee et al. (2006). Therefore, the reproducibility of castings is one of the serious concerns for the HPDC process. Limited researches have addressed the repeatability of die-castings, in particular for the effect of vacuum assisted HPDC on the repeatability. Weibull analysis was reported as a useful measure of the repeatability and reliability of manufacturing processes (Tiryakioğlu and Campbell, 2010; Tiryakioğlu, 2015). In addition, vacuum assisted HPDC can enable the strengthening of die castings through heat treatment, due to the low levels of gas porosities in the castings. However, more evidences are essentially needed to validate the effect of vacuum assisted HPDC on the heat-treated die castings because of the inconsistency of reported results. The generally achieved vacuum levels in literatures for vacuum assisted HPDC were above the critical value of 50 mbar, as reported by Wang et al. (2014). Shi et al. (2012) reported the super vacuum of ~50 mbar during HPDC. Seldom did literatures achieve the super vacuum that is far below the critical value of 50 mbar.

In this investigation, the super vacuum assisted HPDC was achieved with a vacuum level that was far below the critical value of 50 mbar, and the Al-Si-Mg-Mn alloy was die-cast using the super vacuum assisted HPDC in comparison with conventional HPDC. The microstructural characteristics and the assessment of the tensile properties of the alloy were conducted. The repeatability of mechanical properties under as-cast and heat-treated conditions was analysed by Weibull models in order to obtain the quantitative results. The porosity levels were analysed and discussed in association with the tensile properties and repeatability of the alloy.

2. Experimental

2.1. Materials preparation

The Al-Si-Mg-Mn die-cast alloys were melted in the electric resistance furnace, and the alloys for conventional HPDC and super vacuum assisted HPDC were melted in two different crucibles. The alloy was prepared by the addition of the master alloys of Al-50wt.% Si, Al-20wt.% Mn, Al-45wt.% Fe and Al-10wt.% Ti and the pure ingots of Al and Mg. The active element Mg was over added by 5 % for the compensation of its burning during melting. After melting, 200 ppm Sr was added into the melt in the form of Al-10 wt.% Sr master alloy, for the modification of the eutectic Si phase. The rotary degassing impeller was applied for the degassing of the melt, and the rotation speed of the impeller was 350 rpm. Pure argon was injected to the melt during degassing, and the degassing time was 5 min for an amount of 10 kg melt. After degassing, the melt was hold at 720 °C. One mushroom sample was made for each melt for the composition analysis and the results are shown in Table 1, followed by conventional HPDC and super vacuum assisted HPDC.

Table 1 Chemical compositions of the investigated alloys obtained by ICP-AES (wt.%).

Alloy	Si	Mg	Mn	Fe	Ti	Zn	Sr	Al
A1 (Conventional HPDC)	8.86	0.38	0.58	0.15	0.13	0.009	0.02	Bal.
A2 (Super vacuum HPDC)	8.82	0.39	0.57	0.15	0.13	0.008	0.02	Bal.

2.2. Two-stage super vacuum assisted HPDC

A 4500 kN cold chamber HPDC machine equipped with the specially designed two-stage vacuum system was used for the making of standard ASTM tensile samples. As shown in Figs. 1(a) and (b), the vacuum system was set as two stages: one was located at the shot sleeve, and the other was located at the top of die cavity. Different from the commonly used one-stage vacuum by evacuation only from the die cavity, here the two-stage vacuum was conducted by evacuation from both the shot sleeve and the die cavity simultaneously during HPDC, which could achieve higher vacuum level in limited evacuation time. The casting die was preheated at 250 °C by the oil, and the shot sleeve was preheated at 180 °C by the compressed hot water. The melt temperature in the pouring ladle was measured as 690 °C before pouring. Eight ASTM B557 standard tensile samples with a gauge dimension of ϕ6.35 mm × 50 mm were cast by each HPDC shot, see Fig. 1(c).

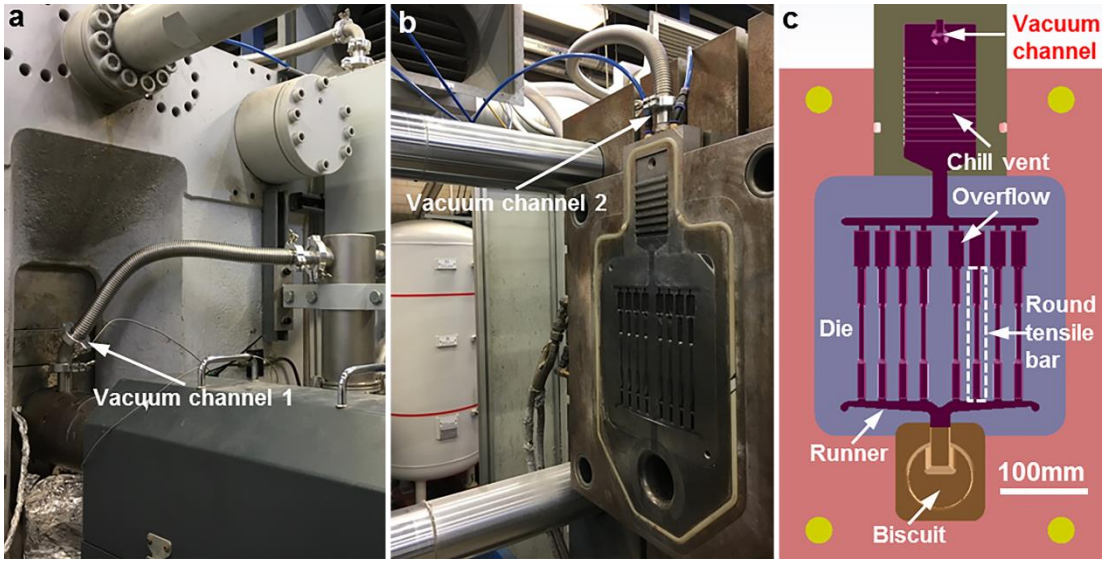

Fig. 1. The setup of two-stage super vacuum assisted HPDC system, (a) one channel at shot sleeve and (b) one channel at the top of die cavity, and (c) the cross section of die-set showing the location of round tensile test samples designed according to ASTM B557.

2.3. Heat treatment and tensile tests

After being left at ambient condition for at least one day, T6 heat treatment was applied to the cast samples, and the T6 heat treatment included the solid solution and the subsequent artificial ageing. The solid solution was conducted at 540 °C for 30 minutes, and then the samples were rapidly quenched after solution. The artificial ageing was carried out at 170 °C for 8 hours. The tensile tests were performed at the ambient temperature on an Instron 5500 machine, according to the standard E8 of ASTM. The extensometer with the gauge length of 50 mm was applied for the monitoring of the strain, and the ramp rate was set as 1 mm/min during tensile tests. More than sixty tensile bars were pulled for each reported situation.

2.4. Microstructure characterization

The Zeiss field emission scanning electron microscope (SEM) and the JEOL-2100 transmission electron microscopy (TEM) were used for the microstructure examination. The standard method of grinding was applied for the preparation of the SEM samples. The polished SEM samples were etched by 15 vol.% hydrochloric acid before SEM observation. The TEM specimens were first ground to the thickness of ~100 μm, and then the further reduction of the TEM specimens was conducted by electropolishing at 20 V and -30 °C. The chemical solution for electropolishing was the methyl alcohol and nitric acid with a ratio of 4:1. The TEM characterization was performed at 200 kV for the imaging of bright field and high-resolution transmission electron microscopy (HRTEM), and the analysis of select area diffraction pattern (SADP). The porosity levels were measured by the density method.

2.5. Weibull statistical analysis

The three-parameter Weibull distribution was applied for the Weibull statistical analysis, and its expression is as follows:

$$P_f = 1 - exp\left[-\frac{\sigma-\sigma_u}{\sigma_0}\right]^m \quad (1)$$

$$\ln\left[\ln\left(\frac{1}{1-P_f}\right)\right] = m[\ln(\sigma-\sigma_u) - \ln\sigma_0] \quad (2)$$

Where P_f represented the accumulated probability of the fracture of the samples during tensile tests; σ was the yield strength, ultimate tensile strength or elongation that was tested during tensile tests; σ_u was the threshold value; σ_0 was the featured stress or strain corresponding to the fracture probability of 63.2%; m was the Weibull modulus. The analysis of linear regression was applied to the data plot of $\ln[\ln(1/(1-P_f))]$ and $\ln(\sigma-\sigma_u)$. The correlation coefficient of the linear regression was R^2. Different R^2 was calculated by the setting of a group of σ_u that were lower than the tested result σ. After the threshold value σ_u was obtained corresponding to the situation that yielded the maximal R^2. The slope m of the regression line that had the maximum R^2 physically represented the Weibull

modulus, and higher Weibull modulus demonstrated higher repeatability and reliability. The *y*-intercept of the linear regression analysis was the featured value σ_0. The rank method was applied for the determination of the P_f as follows:

$$P_f = (i - 0.3)/(n + 0.4) \quad (3)$$

Where *i* was the sequence number of the tested samples, and *n* was the total number of the tested samples.

The critical value of R^2 at α=0.05 ($R^2_{0.05}$) was calculated according to the following formula (Ji et al., 2013), for the evaluation of the compatibility of Weibull distribution.

$$R^2_{0.05} = 1.0637 - \frac{0.4174}{n^{0.3}} \quad (4)$$

In this investigation, *n* was 62, and the critical value $R^2_{0.05}$ was 0.9427. When the R^2 of the tested data was higher than$R^2_{0.05}$, then the tested data agreed with Weibull distribution.

3. Results and discussion

3.1. Vacuum level during HPDC

Fig. 2 shows the evacuation process during the two-stage super vacuum assisted HPDC. At time T1, the head of the plunger just passed the feeding inlet of the shot sleeve, and the evacuation of the shot sleeve and the die cavity started due to the seal of the system. At time T2, the head of the plunger started passing the vacuum channel 1 in the shot sleeve. From time T1 to T2, the evacuation was conducted simultaneously from the vacuum channel 1 in the shot sleeve and the vacuum channel 2 on the top of the die cavity. After time T2, the head of the plunger passed the vacuum channel 1 and the vacuum channel 1 stopped evacuating. From time T2 to T3, the evacuation only relied on the vacuum channel 2. From time T3 to T4, the high speed shot and filling of the die cavity happened under super vacuum.

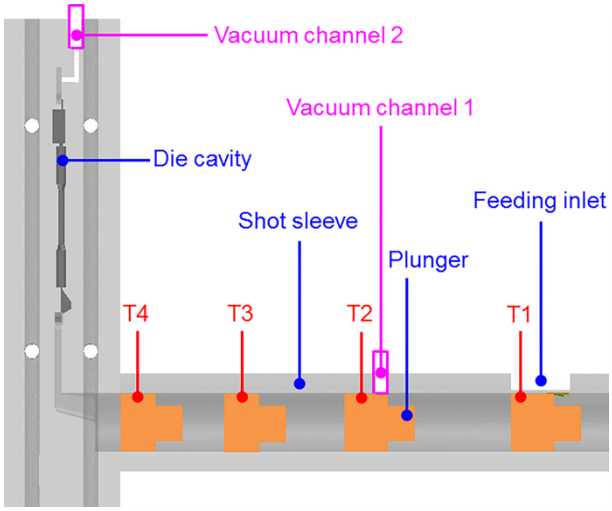

Fig. 2. The evacuation process during the two-stage super vacuum assisted high pressure die casting.

Fig. 3 shows the actual vacuum level during the super vacuum assisted HPDC. At time T1, the vacuum level in the shot sleeve and the die cavity was at the standard atmosphere of ~1000 mbar. From time T1 to T2, the vacuum level in the die cavity and shot sleeve decreased sharply due to the evacuation. At time T2, the vacuum level in the shot sleeve decreased to the local minimum level of 35 mbar, while the vacuum level in the die cavity decreased to 250 mbar. After time T2, the vacuum level in the later part of the shot sleeve returned immediately to the standard atmosphere due to the release of the seal. At time T3, the vacuum level in the die cavity decreased to the minimum of 19 mbar. The vacuum level of 19 mbar was super vacuum as 50 mbar was usually considered as the critical value of super vacuum for HPDC. From time T3 to T4, the die cavity kept at the super vacuum of 19 mbar during high speed shot and rapid solidification. The present achieved super vacuum of 19 mbar under the two-stage evacuation process was much lower than the super vacuum of ~50 mbar that was reported previous by Shi et al. (2012), and also significantly lower than the vacuum of 100-800 mbar that was reported previous by Wang et al. (2014). A vacuum of 34 mbar was obtained under the condition of the one-stage evacuation just from the die cavity, so the two-stage evacuation process could improve the vacuum level by 15 mbar over the one-stage evacuation process on this machine.

Thus, the two-stage evacuation from both the shot sleeve and die cavity ensured the super vacuum of 19 mbar in the very limited evacuation time during HPDC.

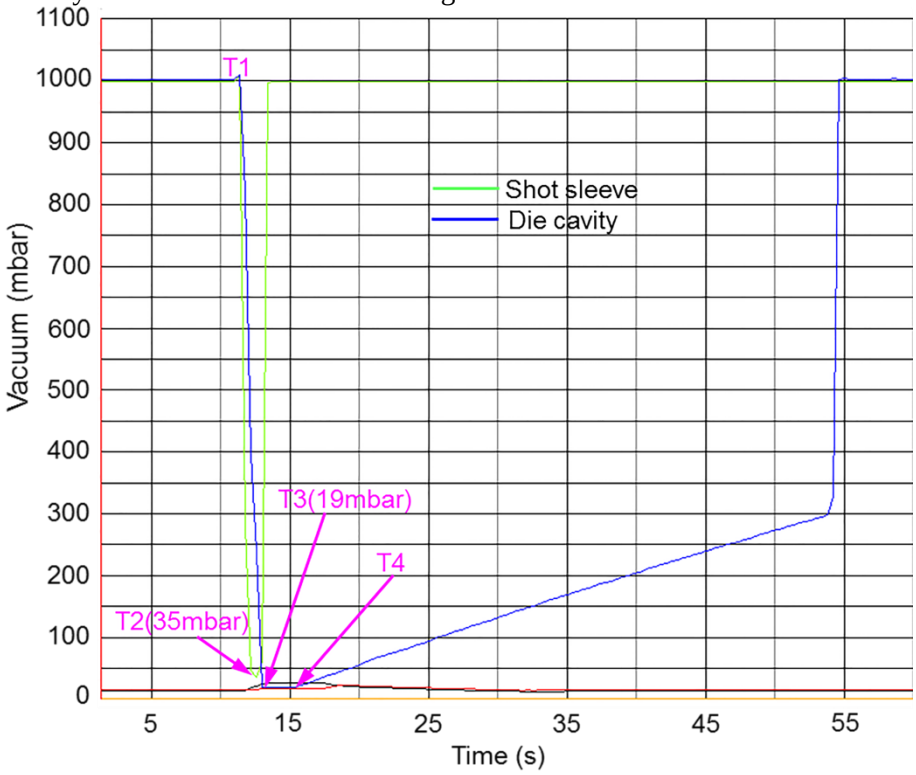

Fig. 3. The vacuum level during the two-stage super vacuum assisted high pressure die casting.

3.2. Tensile properties

Fig. 4 presents the representative tensile stress-strain curves of the Al-Si-Mg-Mn die-cast alloy made by conventional HPDC and super vacuum assisted HPDC. For the as-cast alloy, although the yield strength under conventional HPDC was very close to that obtained by super vacuum assisted HPDC, the ultimate tensile strength (UTS) and the ductility were obviously different. The super vacuum assisted HPDC could increase the UTS and elongation. It was noted that the strain strengthening was over 130 MPa during the plastic deformation stage. For the T6 heat-treated alloy, the yield strength and UTS under conventional HPDC were similar with that obtained from super vacuum assisted HPDC, while the elongation of the alloy made by super vacuum assisted HPDC was higher than that made by conventional HPDC. However, the strain strengthening during plastic deformation stage was only 60 MPa, which confirmed that the strain strengthening effect in the T6 state was not as significant as that in the as-cast state.

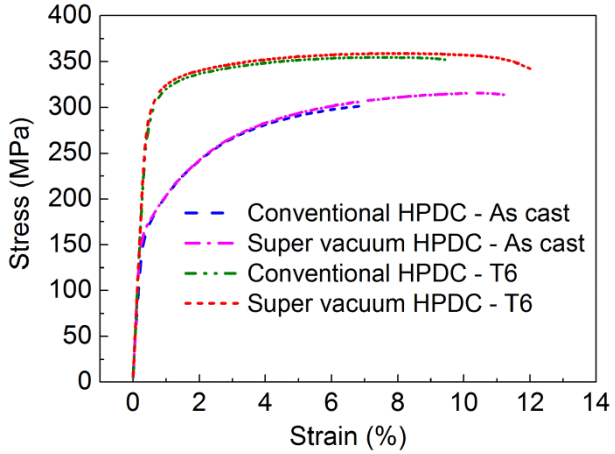

Fig. 4. Representative tensile stress-strain curves of the Al-Si-Mg-Mn alloy processed by conventional HPDC and super vacuum assisted HPDC under as-cast and T6 heat-treated states.

Fig. 5 presents the distribution of tensile properties and Table 2 summaries the measured data of the Al-Si-Mg-Mn alloy processed by conventional HPDC and super vacuum assisted HPDC, respectively. For the as-cast alloy, the yield strength was 167.7±2.4 MPa under conventional HPDC and that was 169.5±1.6 MPa under super vacuum assisted HPDC, indicating that the super vacuum assisted HPDC does not have a significant influence on the yield strength. However, the super vacuum assisted HPDC was very helpful to improve the UTS and ductility of the alloy in as-cast state. The UTS was 300.9±10.0 MPa for the alloy processed by conventional HPDC and 317.6±1.4 MPa for the alloy processed by super vacuum assisted HPDC in which the increase was 5.6 %. The elongation was 8.1±2.1 % for the alloy processed by conventional HPDC and 11.6±0.7 % for the alloy processed by super vacuum assisted HPDC, resulting in the obvious increase of 43 %. Moreover, it was found that the fluctuation of the elongation in the as-cast alloy was significantly reduced under super vacuum assisted HPDC. The as-cast elongation measured for conventional HPDC samples fluctuated between 4.9 % and 12.9 %, while that for super vacuum assisted HPDC fluctuated between 10.7 % and 13.0 %. Therefore, the super vacuum assisted HPDC reduced the fluctuation of the tensile ductility of the as-cast alloy by 71 %. In addition, the standard deviation of the UTS and the tensile ductility of the as-cast alloy made by super vacuum assisted HPDC decreased by 86 % and 67 %, respectively, when compared with the alloy made by conventional HPDC.

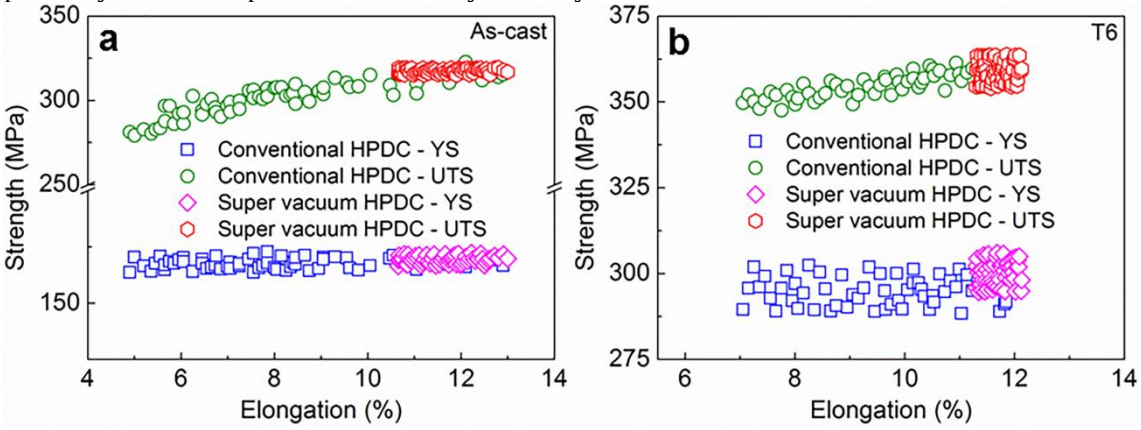

Fig. 5. Distribution of the tensile properties of the Al-Si-Mg-Mn alloy processed by conventional HPDC and super vacuum assisted HPDC: (a) as-cast state and (b) T6 state.

In T6 heat-treated state, the alloy made by conventional HPDC provided the yield strength of 297.1±4.3 MPa, the UTS of 355.3±3.7 MPa and the elongation of 9.7±1.5 %. The alloy processed by super vacuum assisted HPDC provided the yield strength of 300.2±3.4 MPa, the UTS of 359.0±3.1 MPa and the elongation of 11.7±0.3 %. Thus the yield strength of the alloy after T6 heat treatment was not obviously influenced by the process of super vacuum assisted HPDC, although it was doubled the value that was obtained under as-cast condition. However, the elongation was significantly affected by the process. The elongation increased considerably by 21 % under super vacuum assisted HPDC. Moreover, the fluctuation of the elongation in the T6 heat-treated alloy was also significantly reduced under super vacuum assisted HPDC. The T6 heat-treated elongation measured for conventional HPDC samples fluctuated between 7.0 % and 11.9 %, while that for super vacuum assisted HPDC fluctuated between 11.3 % and 12.1 %. The super vacuum assisted HPDC could also result in the considerable decrease of the fluctuation by 84 % for the ductility of the alloy, after T6 heat treatment. Furthermore, the super vacuum assisted HPDC could decrease the standard deviation of the ductility of the T6 heat-treated alloy by 80 %, when compared with the conventional HPDC.

Table 2 The tensile properties of the Al-Si-Mg-Mn die-cast alloy under different HPDC and heat treatment conditions.

State	Process	Elongation (%)		YS (MPa)		UTS (MPa)	
		Average	2xSTDEVA	Average	2xSTDEVA	Average	2xSTDEVA
As-cast	Conventional HPDC	8.1	2.1	167.7	2.4	300.9	10.0
	Super vacuum HPDC	11.6	0.7	169.5	1.6	317.6	1.4

T6	Conventional HPDC	9.7	1.5	297.1	4.3	355.3	3.7
	Super vacuum HPDC	11.7	0.3	300.2	3.4	359.0	3.1

3.3. Weibull analysis and repeatability

The measured tensile properties of strength and ductility were organised in the ascending order, and P_f was calculated from Eq. (3). Figs. 6(a) shows the example of Weibull plots for the as-cast tensile elongation of the investigated alloy processed by conventional HPDC. The slope of the fitting line in Fig. 6(a) was the Weibull modulus m. The threshold parameter Elu, scaling parameter El_0 and R^2 were determined through the equations, by which the coefficient of correlation R^2 for the linear regression can be obtained and shown in Fig. 6(b). The maximum R^2 and the associated parameters were taken as the results of Weibull analysis. Using the same method, all the Weibull parameters were obtained for the tensile strength and ductility.

Table 3 lists the results of Weibull analysis. From Table 3, the coefficient of correlation R^2 of the linear regression of the yield strength was much less than the critical value of 0.9427. Therefore, the as-cast yield strength of the investigated alloy processed by conventional HPDC and super vacuum assisted HPDC did not follow the Weibull distribution, which also confirmed that the yield strength was not determined by "weakest link". In the meantime, the results showed that the UTS and the tensile elongation followed the Weibull distribution since all of the corresponding values of R^2 were higher than the critical value of 0.9427.

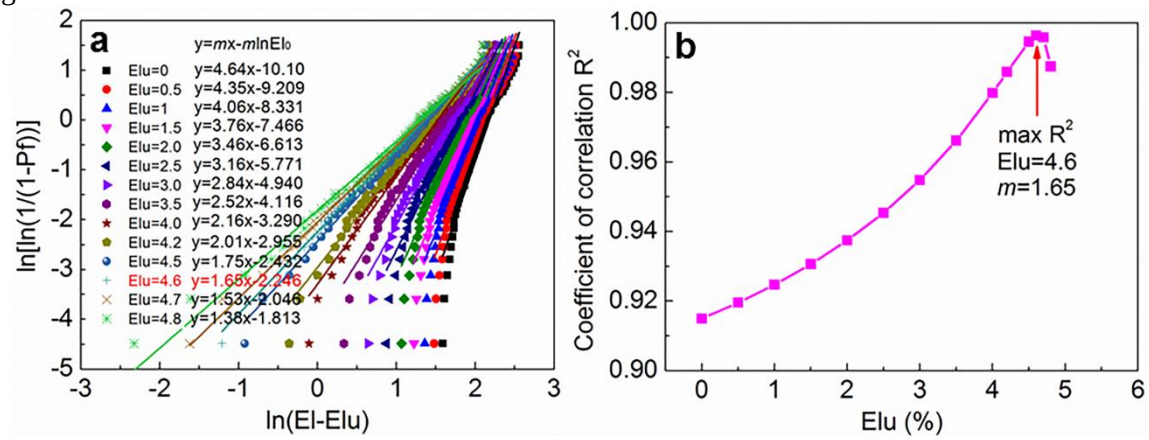

Fig. 6. The example of Weibull plots for the (a) as-cast elongation of the Al-Si-Mg-Mn alloy under conventional HPDC, and (b) the corresponding coefficient of correlation R^2.

Table 3 Calculated results for the Weibull parameters of the tensile properties of the Al-Si-Mg-Mn alloy under different conditions.

Property	Process	State	m	σ_u	σ_0	R^2
YS	Conventional HPDC	As-cast	-	163	-	0.032
		T6	-	286	-	0.010
	Super vacuum HPDC	As-cast	-	166	-	0.147
		T6	-	260	-	0.183
UTS	Conventional HPDC	As-cast	2.28	275	29.68	0.974
		T6	2.45	346	10.58	0.990
	Super vacuum HPDC	As-cast	2.53	314	4.02	0.951
		T6	2.80	351	8.93	0.956
Elongation	Conventional HPDC	As-cast	1.65	4.6	3.90	0.996
		T6	1.93	6.6	3.58	0.974
	Super vacuum HPDC	As-cast	2.26	10.2	1.63	0.964
		T6	2.59	11.1	0.67	0.971

From Table 3, the Weibull modulus *m* of the UTS and ductility of the Al-Si-Mg-Mn alloy processed by super vacuum assisted HPDC was higher than that processed by conventional HPDC, which verified that super vacuum assisted HPDC could provide higher repeatability of the die-castings than the conventional HPDC. Meanwhile, the super vacuum assisted HPDC provided higher threshold and lower scaling parameters compared to the conventional HPDC. Therefore, the tensile strength and elongation are enhanced under the process of super vacuum assisted HPDC.

3.4. Microstructure

Figs. 7(a,b) and (c,d) show the as-cast SEM morphology of the Al-Si-Mg-Mn alloy processed by conventional HPDC and super vacuum assisted HPDC, respectively. Two kinds of α-Al phase were found in the alloy, i.e., the primary α_1-Al phase nucleated from the shot sleeve and the secondary α_2-Al phase nucleated from the cavity of die. The α_2-Al phase is much smaller than the α_1-Al phase because of the higher cooling rate of solidification in the die, as reported by Dong et al. (2019). The eutectic phase of Si and the intermetallic phase of β-Mg_2Si were also identified in the microstructure. The eutectic Si phase was in fibrous shape. The β-Mg_2Si phase was located in the Al-Si eutectic region, and it is in blocky shape. There is not much difference for the phases in the as-cast alloy processed by conventional HPDC and super vacuum assisted HPDC, confirming that super vacuum assisted HPDC does not have significant influence on the formation of phases in the die-castings.

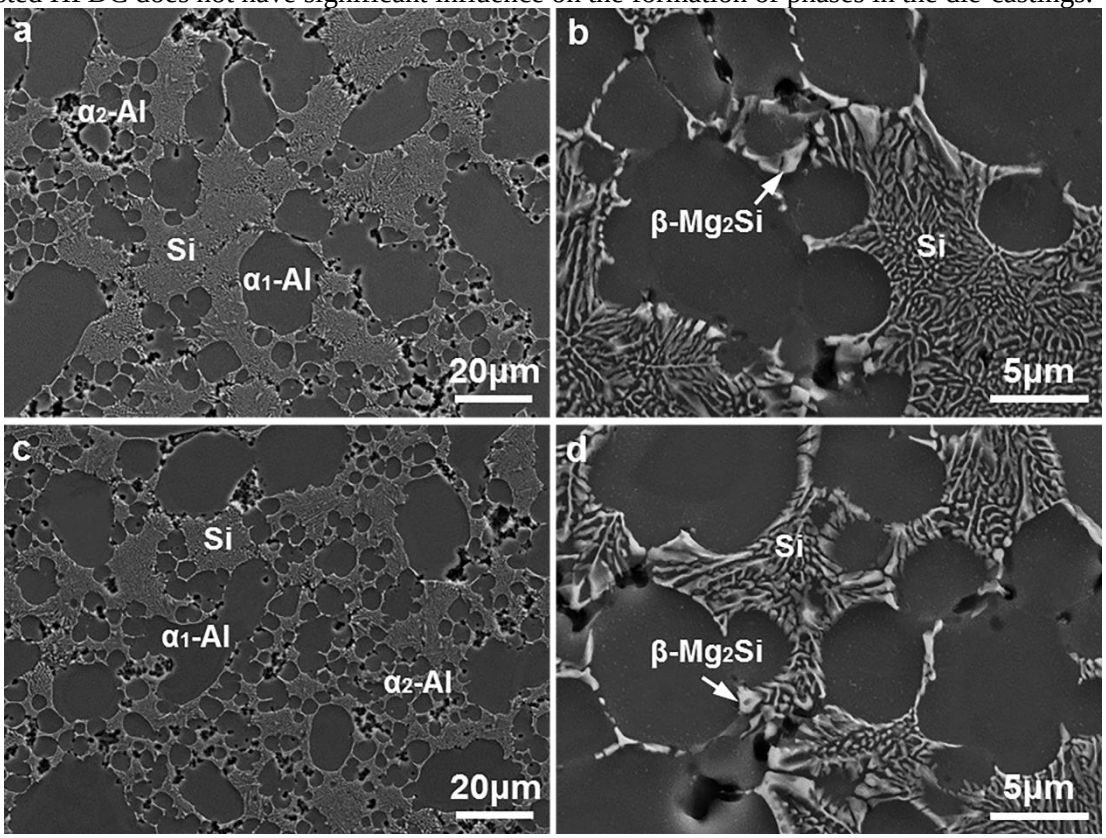

Fig. 7. The as-cast SEM morphology of the Al-Si-Mg-Mn alloy processed by (a,b) conventional HPDC and (c,d) super vacuum assisted HPDC.

Figs. 8(a,b) and (c,d) present the SEM images of the Al-Si-Mg-Mn alloy processed by conventional HPDC and super vacuum assisted HPDC, respectively, after T6 heat treatment. The Al phase was slightly coarsened after T6 heat treatment, when compared with the as-cast situation. After T6 heat treatment, the Si phase was changed into the spheroidal shape. In addition, the β-Mg_2Si phase disappeared in the T6 heat-treated microstructure, which demonstrated the good dissolving of the β-Mg_2Si phase during the solid solution. The super vacuum assisted HPDC does not have significant impact on the change of phases in the alloy during T6 heat treatment. The T6 heat-treated alloys have a smaller distribution in ductility when compared to the as-cast alloys, for the conditions of both super vacuum HPDC and conventional HPDC, as shown in Fig. 5. This was the case because no blistering occurred during the solution treatment of the alloys processed by conventional HPDC in this work, and the relatively short solution time of 30 minutes contributed to the non-occurring of the blistering.

The spheroidization of the eutectic Si phase and the solid solution of the intermetallic phase after solution treatment contribute to the smaller distribution in ductility in T6 heat-treated alloys. With the occurring of blistering during the solution treatment of some conventionally HPDC alloys other than the condition in this work, the distribution of ductility in the T6 heat-treated alloys might be expected larger than the as-cast alloys.

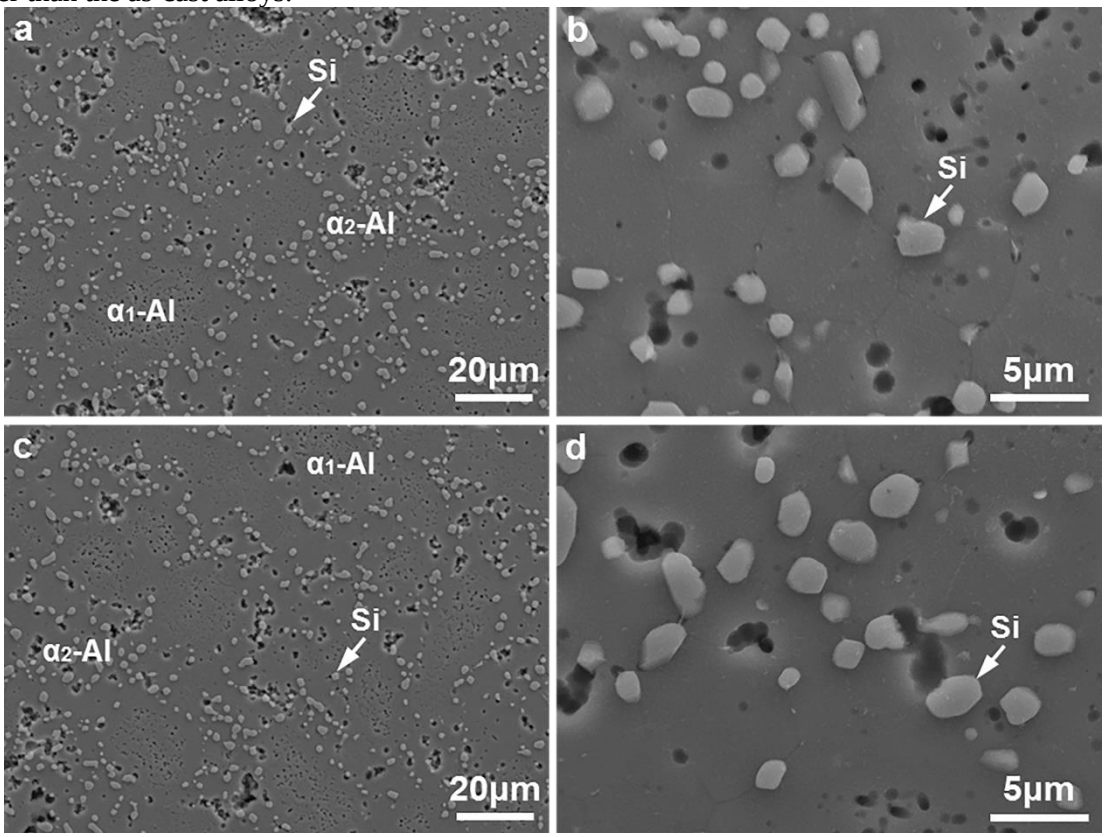

Fig. 8. SEM morphology of the Al-Si-Mg-Mn alloy processed by (a,b) conventional HPDC and (c,d) super vacuum assisted HPDC after T6 heat treatment.

The β-Mg_2Si phase was dissolved into the α-Al matrix during solution treatment, and it was expected to be precipitated in the form of β" precipitates for the strengthening of the Al matrix after ageing treatment. The TEM images in Fig. 9 show the precipitate in the Al-Si-Mg-Mn die-cast alloy after solution and ageing treatment, which were taken from the zone axis of $<001>_{Al}$. From the bright field TEM image shown in Fig. 9(a), the β" precipitates were observed embedding and lying in the Al matrix. The embedded and lying β" precipitates were the same β" precipitates in nature (Dong et al., 2018), as the β" precipitate was in the needle-like shape. The SADP in Fig. 9(b) indicated the presence of the β" precipitates in the Al matrix. The HRTEM image in Fig. 9(c) presents the exact atomic structure of the embedded β" precipitate, and it verified that the precipitate was β", as reported by Andersen et al. (1998). The FFT image in Fig. 9(d) also confirmed the precipitate in Fig. 9(c) was β" (Dong et al., 2018). The β" precipitates would provide the peak strengthening (Dong et al., 2017).

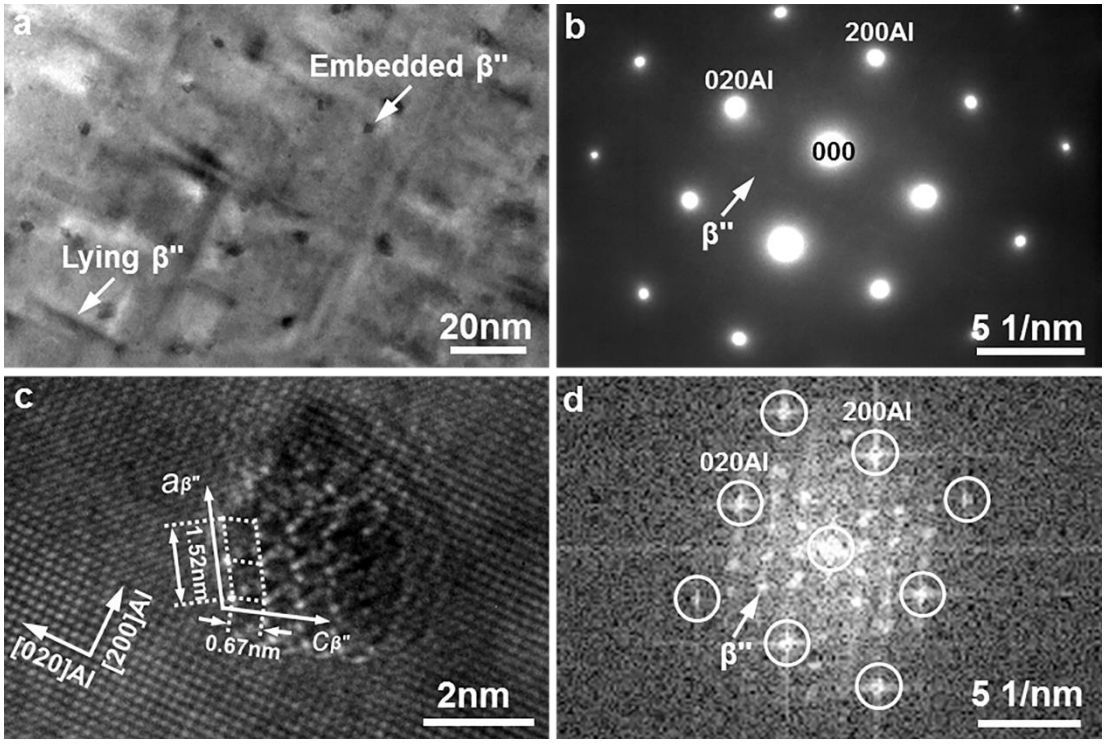

Fig. 9. TEM images presenting the precipitation strengthening in the Al-Si-Mg-Mn alloy processed by HPDC after T6 heat treatment: (a) morphology of precipitate, (b) diffraction pattern of the matrix and the precipitate, (c) high resolution image of the precipitate, (d) FFT of the precipitate in (c).

3.5. Morphology of fracture

Figs. 10(a,b) and (c,d) present the typical as-cast SEM morphology of the fracture of the Al-Si-Mg-Mn alloy processed by conventional HPDC and super vacuum assisted HPDC, respectively. As indicated by the arrows in Figs. 10(b,d), the size of the gas porosity in the fracture of the alloy processed by super vacuum assisted HPDC was decreased significantly, when compared with the alloy processed by conventional HPDC. The largest size of the gas porosity in the fracture of the alloy processed by super vacuum assisted HPDC was measured as 155 μm, while the largest size of the gas porosity in the fracture of the alloy processed by conventional HPDC was decreased obviously to 21 μm. No difference was found for the morphology of fracture in the non-porosity area of the alloy processed by conventional and super vacuum assisted HPDC. Thus, the fracture of the investigated die-cast alloy was controlled by the porosity. The obvious reduction of porosity size resulted in the considerable improvement of elongation in the investigated die-cast alloy processed by super vacuum assisted HPDC.

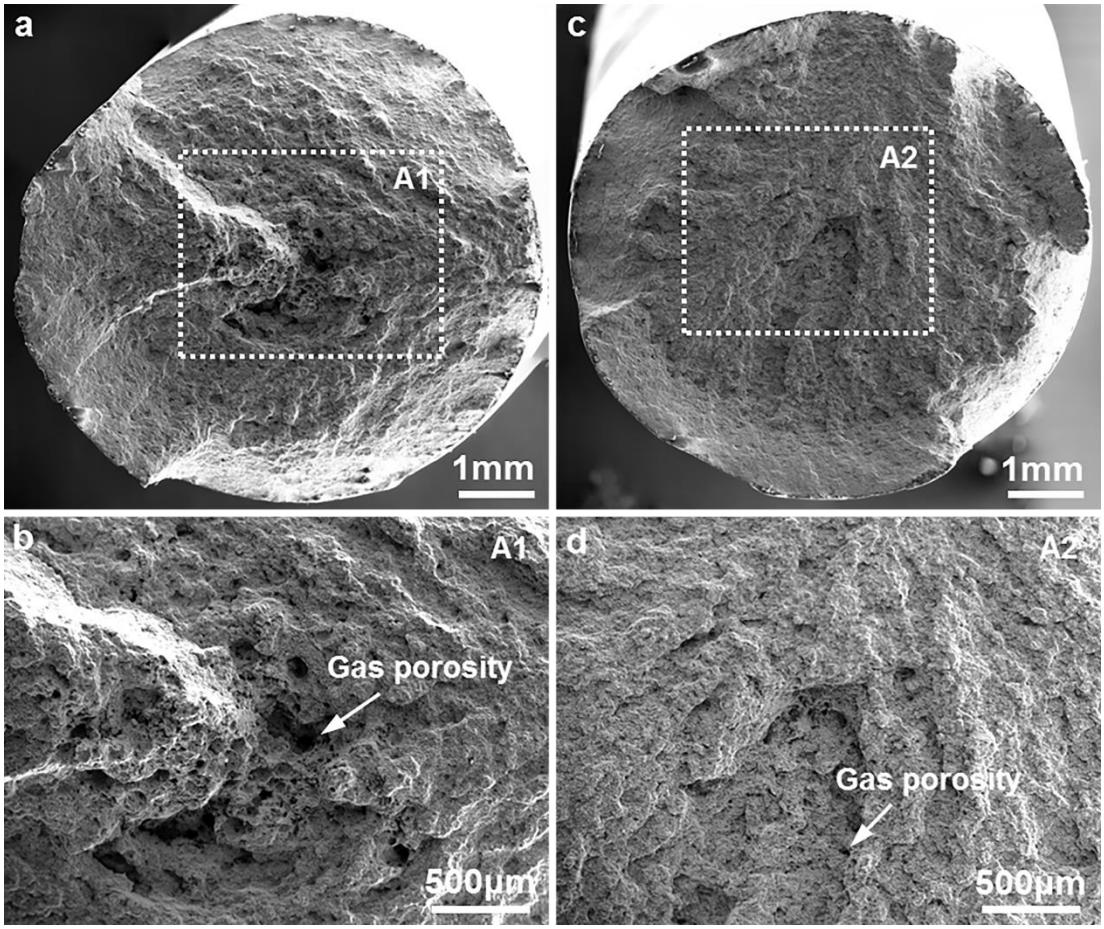

Fig. 10. Typical as-cast fracture surface of the Al-Si-Mg-Mn die-cast alloy processed by (a,b) conventional HPDC and (c,d) super vacuum assisted HPDC.

3.6. Porosity level

Fig. 11 presents the measured porosity levels in the as-cast Al-Si-Mg-Mn die-cast alloy processed by conventional HPDC and super vacuum assisted HPDC. The porosity level of the as-cast alloy processed by super vacuum assisted HPDC was significantly decreased by 90 % to 0.08 %, when compared with the alloy that was processed by conventional HPDC. Thus, super vacuum assisted HPDC could significantly decrease the porosity level in the investigated die-cast alloy.

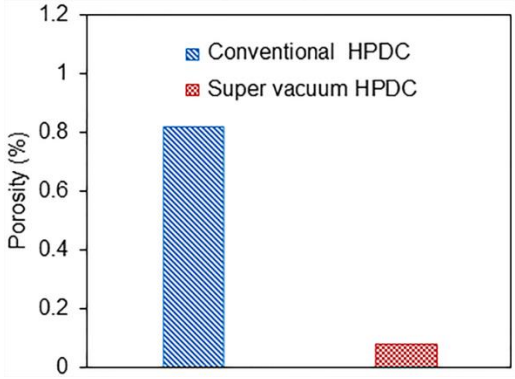

Fig. 11. Comparison of porosity levels in the as-cast Al-Si-Mg-Mn alloy processed by conventional HPDC and super vacuum assisted HPDC.

The decrease of porosity level and size resulted in the improvement of strength under super vacuum assisted HPDC. From Fig. 10, the counted number of porosity in the fracture of the die-cast alloy processed by conventional and super vacuum assisted HPDC were 395 and 360, respectively. So super vacuum assisted HPDC did not decrease the number of porosity significantly. However, super vacuum assisted HPDC obviously decreased the size of porosity on the fracture surface, when compared with conventional HPDC. This resulted in the weak and even distribution of stress

concentration under external load. Thus, the ability to resist the external load was enhanced and the discrepancy between the die-castings was decreased, which leaded to the improvement of the strength, ductility and repeatability of the die-castings. The ductility of the cast alloys was dependent on the area fraction and size of the defect in the fracture, as reported by Surappa et al. (1986) and Cáceres et al. (1996). The initiation of cracks could be retarded in the samples with much less defect size, and it resulted in the improvement of the ductility of the die-cast alloy processed by super vacuum assisted HPDC. The decrease of porosity size and area fraction increased the effective area under external load, and it decreased the probability and uncertainty of failure during deformation. This decreased the fluctuation of the measured tensile properties, which corresponded to the improvement of repeatability. Thus, the super vacuum HPDC process is very helpful to improve the repeatability of the die-castings.

4. Conclusions

(1) Super vacuum level of 19 mbar was achieved for HPDC by the setting of two-stage evacuation from the shot sleeve and the die cavity simultaneously.

(2) Super vacuum assisted HPDC improves the ductility of the Al-Si-Mg-Mn die-cast alloy comparing with conventional HPDC. The ductility is increased by 43 % in as-cast state, and the ductility is enhanced by 21 % after T6 heat treatment.

(3) Super vacuum assisted HPDC reduces the fluctuation of the ductility of the Al-Si-Mg-Mn die-cast alloy comparing with conventional HPDC. The fluctuations of the ductility are decreased by 71 % in as-cast state and 84 % after T6 heat treatment.

(4) Super vacuum assisted HPDC improves the repeatability of the tensile properties of the Al-Si-Mg-Mn die-cast alloy comparing with conventional HPDC.

(5) Super vacuum assisted HPDC decreases the porosity level and porosity size in the as-cast Al-Si-Mg-Mn alloy comparing with conventional HPDC, which leads to the improvement of the tensile strength, ductility and their repeatability.

Acknowledgements

Innovate UK is acknowledged for the support of the work.

References

Andersen, S.J., Zandbergen, H.W., Jansen, J., Traeholt, C., Tundal, U., Reiso, O., 1998. The crystal structure of the β" phase in Al-Mg-Si alloys. Acta Mater. 46, 3283-3298.

Cao, H.X., Hao, M.Y., Shen, C., Liang, P., 2017. The influence of different vacuum degree on the porosity and mechanical properties of aluminum die casting. Vacuum 146, 278-281.

Cáceres, C.H., Selling, B.I., 1996. Casting defects and the tensile properties of an Al-Si-Mg alloy. Mater. Sci. Eng. A 220, 109-116.

Dong, X.X., He, L.J., Huang, X.S., Li, P.J., 2015. Coupling analysis of the electromagnetic transport of liquid aluminum alloy during casting. J. Mater. Process. Technol. 222, 197-205.

Dong, X.X., He, L.J., Huang, X.S., Li, P.J., 2015. Effect of electromagnetic transport process on the improvement of hydrogen porosity in A380 aluminum alloy. Int J Hydrogen Energy 40, 9287-9297.

Dong, X.X., Huang, X.S., Liu, L.H., He, L.J., Li, P.J., 2016. A liquid aluminum alloy electromagnetic transport process for high pressure die casting. J. Mater. Process. Technol. 234, 217-227.

Dong, X.X., Ji, S.X., 2018. Si poisoning and promotion on the microstructure and mechanical properties of Al-Si-Mg cast alloys. J Mater. Sci. 53, 7778-7792.

Dong, X.X., Yang, H.L., Zhu, X.Z., Ji, S.X., 2019. High strength and ductility aluminium alloy processed by high pressure die casting. J. Alloys Compd. 773, 86-96.

Dong, X.X., Zhang, Y.J., Amirkhanlou, S., Ji, S.X., 2018. High performance gravity cast Al9Si0.45Mg0.4Cu alloy inoculated with AlB_2 and TiB_2. J. Mater. Process. Technol. 252, 604-611.

Dong, X.X., Zhang, Y.J., Ji, S.X., 2017. Enhancement of mechanical properties in high silicon gravity cast AlSi9Mg alloy refined by Al3Ti3B master alloy. Mater. Sci. Eng. A 700, 291-300.

Ji, S., Yang, W., Jiang, B., Patel, J.B., Fan, Z., 2013. Weibull statistical analysis of the effect of melt conditioning on the mechanical properties of AM60 alloy. Mater. Sci. Eng. A 566, 119-125.

Lee, S.G., Patel, G.R., Gokhale, A.M., Sreeranganathan, A., Horstemeyer, M.F., 2006. Quantitative fractographic analysis of variability in the tensile ductility of high-pressure die-cast AE44 Mg-alloy. Mater. Sci. Eng. A 427, 255-262.

Li, X., Xiong, S.M., Guo, Z., 2016. Correlation between porosity and fracture mechanism in high pressure die casting of AM60B alloy. J. Mater. Sci. Technol. 32, 54-61.

Li, X., Xiong, S.M., Guo, Z., 2016. Improved mechanical properties in vacuum-assist high-pressure die casting of AZ91D alloy. J. Mater. Process. Technol. 231, 1-7.

Niu, X.P., Hu, B.H., Pinwill, I., Li, H., 2000. Vacuum assisted high pressure die casting of aluminium alloys. J. Mater. Process. Technol. 105, 119-127.

Patel, H.A., Rashidi, N., Chen, D.L., Bhole, S.D., Luo, A.A., 2012. Cyclic deformation behavior of a super-vacuum die cast magnesium alloy. Mater. Sci. Eng. A 546, 72-81.

Shi, X.Y., Li, D.J., Luo, A.A., Hu, B., Li, L., Zeng, X.Q., Ding, W.J., 2013. Microstructure and mechanical properties of Mg-7Al-2Sn alloy processed by super vacuum die-casting. Metall. Mater. Trans A 44, 4788-4799.

Surappa, M.K., Blank, E.W., Jaquet, J.C., 1986. Effect of macro-porosity on the strength and ductility of cast Al-7Si-0.3Mg alloy. Scr. Metall. 20, 1281-1286.

Tiryakioğlu, M., 2015. Weibull analysis of mechanical data for castings II: Weibull mixtures and their interpretation. Metall. Mater. Trans A 46, 270-280.

Tiryakioğlu, M., Campbell, J., 2010. Weibull analysis of mechanical data for castings: a guide to the interpretation of probability plots. Metall. Mater. Trans A 41, 3121-3129.

Wan, L., Hu, Z.Q., Wu, S.S., Liu, X.Q., 2013. Mechanical properties and fatigue behavior of vacuum-assist die cast AlMgSiMn alloy. Mater. Sci. Eng. A 576, 252-258.

Wang, L.H., Turnley, P., Savage, G., 2011. Gas content in high pressure die castings. J. Mater. Process. Technol. 211, 1510-1515.

Wang, Q.L., Xiong, S.M., 2014. Vacuum assisted high-pressure die casting of AZ91D magnesium alloy at different slow shot speeds. Trans. Nonferrous Met. Soc. China 24, 3051-3059.

Wang, X.J., Zhu, S.M., Easton, M.A., Gibson, M.A., Savage, G., 2014. Heat treatment of vacuum high pressure die cast magnesium alloy AZ91. Int J Cast Metal Res. 27, 161-166.

Wen, W., Luo, A.A., Zhai, T.G., Jin, Y., Cheng, Y.T., Hoffmann, I., 2012. Improved bending fatigue and corrosion properties of a Mg-Al-Mn alloy by super vacuum die casting. Scr. Mater. 67, 879-882.